ARKIV FÖR FYSIK Band 19 nr 1

Communicated 1 June 1960 by E. Hulthén

Rotational analysis of the blue-green and orange systems of yttrium oxide

By U. Uhler and L. Åkerlind

With 6 figures in the text

ABSTRACT

The blue-green and the orange systems of YO have been photographed at high dispersion. Rotational analysis of the 0,0 bands of both systems has been carried out. The analysis conforms with the earlier assumption that the systems represent a $^2\Sigma$–$^2\Sigma$ and a $^2\Pi$–$^2\Sigma$ transition respectively. The lower states of the systems are identical ($X\,^2\Sigma$). The upper state of the blue-green system ($B\,^2\Sigma$) shows a very large spin-splitting. The upper state of the orange system $A\,^2\Pi$ belongs to Hund's case *a*. The constants are:

State	B_0 cm^{-1}	D_0 cm^{-1}	r_0 cm
B	0.3722	0.38×10^{-6}	1.828×10^{-8}
A	0.3857	0.35×10^{-6}	1.795×10^{-8}
X	0.3881	0.32×10^{-6}	1.790×10^{-8}

$B\,^2\Sigma$–$X\,^2\Sigma$: $\gamma' = 0.148$ cm^{-1} $\sigma_{00} = 20741.92$ cm^{-1}
$A\,^2\Pi_{1/2}$–$X\,^2\Sigma$: $a = 0.151$ cm^{-1} $\sigma_{00} = 16294.72$ cm^{-1}
$A\,^2\Pi_{3/2}$–$X\,^2\Sigma$: $\sigma_{00} = 16722.75$ cm^{-1}

The multiplet splitting constant $A = 428.03$ cm^{-1}.

Introduction

The molecule of YO has two well-known band systems in the visible region. W. F. Meggers and J. A. Wheeler [1] and L. W. Johnson and R. C. Johnson [2] have performed extensive vibrational analyses. Johnson and Johnson have classified more than 100 band heads in five systems designated I–V. After discussing these, they finally conclude that systems I and III and systems II and IV were the two parts of a $^2\Pi$(case *a*)–$^2\Sigma$ transition. The heads of system I are related to those of system III as Q-branches to R-branches, and the heads of system II are analogously related to those of system IV. Johnson and Johnson identify system V as a $^2\Sigma$–$^2\Sigma$ transition with the lower state in common with the $^2\Pi$–$^2\Sigma$ transition.

The present paper gives the rotational analysis of the 0,0 bands of the two systems.

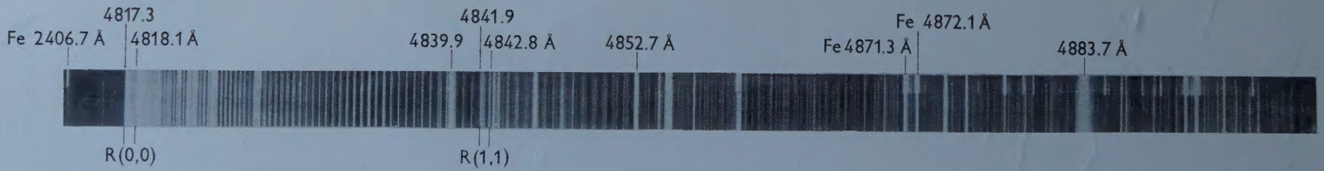

Fig. 1*a*. The 0,0 band of $B^2\Sigma$–$X^2\Sigma$.

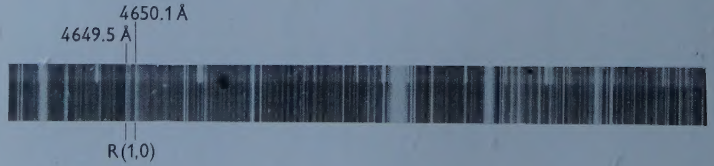

Fig. 1*b*. The 1,0 band of $B^2\Sigma$–$X^2\Sigma$.

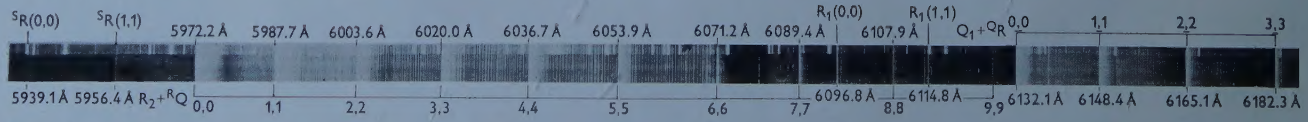

Fig. 2. The band system $A\,^2\Pi(a)$–$X\,^2\Sigma$. The black region between the (6,6) and (7,7) bands is due to a juxtaposition of the photographic plates.

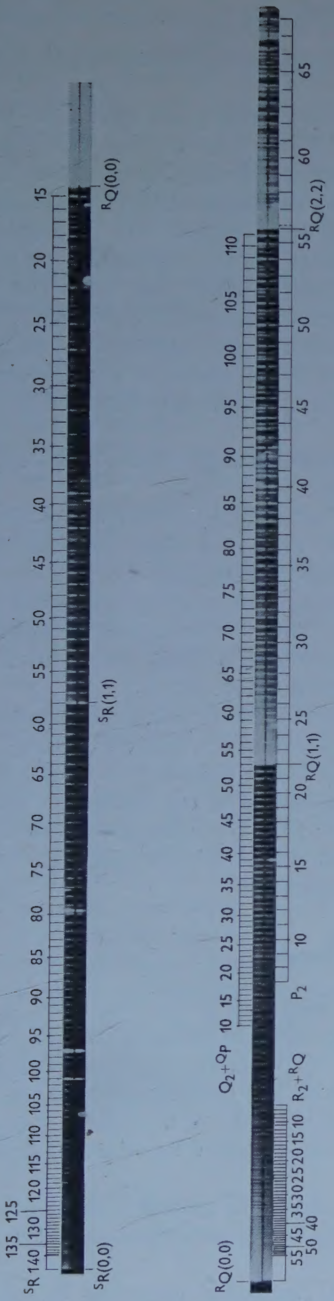

Fig. 3*a*. Rotational structure of the 0,0 band of $A\,^2\Pi_{3/2}$–$X\,^2\Sigma$.

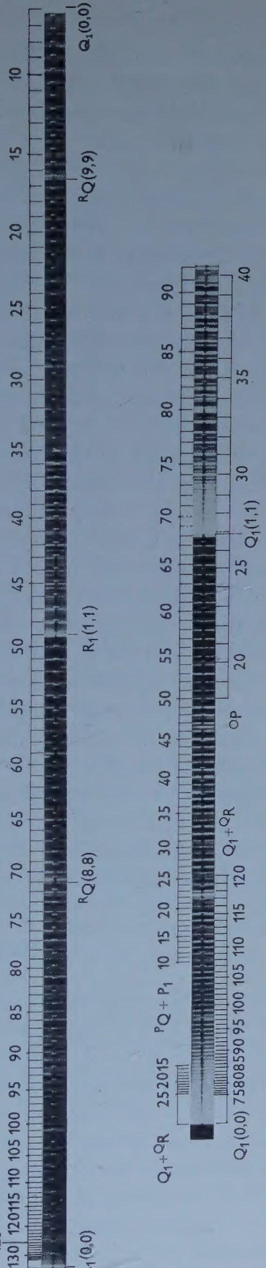

Fig. 3*b*. Rotational structure of the 0,0 band of $A\,^2\Pi_{1/2}$–$X\,^2\Sigma$.

Experimental

The experimental material of the present investigation consists of photographic exposures of the two band systems.

The investigation of this problem was started several years ago. The bands were photographed in a first order of a Wood's 21 ft concave grating, the dispersion of which is about 1.2 Å mm^{-1}. Owing to the extreme density of the structure of the $^2\Pi$–$^2\Sigma$ system the analysis failed. Thanks to the existence of the immersion spectrograph at the institute we were able to resume the study of YO. The spectrograph constructed by Professor Erik Hulthén consists of an aluminized plane replica-grating with 300 grooves mm^{-1} and a "ruled" area of 204 × 106 mm^2. The grating is brought into optical contact with the hypotenuse surface of a 30°/60° flint prism of a somewhat smaller size than the grating with α-brome naphthalene as immersion oil. A telescope lens of 6 m focal length is used in combination with the grating for autocollimation. Further information on the immersion spectrograph is given by Hulthén and co-workers in [3] and [4].

Using the spectrograph in the blazed 60° diffraction angle, one obtains a dispersion of ~ 0.14 Å mm^{-1} in the orange spectral region.

In spite of the coarse ruling of the grating, its resolving power and dispersion are very good, as the maximum intensity of light falls in a high order of the blazed grating. Since the dispersion is very large and no overlapping of orders occurs, there is some difficulty in performing accurate wave-length determination, as the standards lines of Fe and Ne are sparsely distributed. The wave-number determination is therefore made with the aid of interference fringes from a Fabry–Perot interferometer exposed with parallel light from a zirconium-oxide lamp [4].

The blue-green system was photographed in the Wood grating mentioned above. The source of light was an air-acetylene flame [5] fed with a 0.05 m $Y(NO)_3)_3$ solution. The exposure time on Zenith plates was 8 hours. Iron lines served from comparison.

The spectrograms of the orange system were taken in the immersion grating. As the intensity of the flame was too low, we had to use a carbon arc (440V D.C., 15A) whose lower electrode contained $Y(NO_3)_3$. Thin film half-tone panchromatic plates were used and the exposure time was 30–60 minutes.

Structure of bands

The structure of the blue-green 0,0 band is seen in Fig. 1*a*. The band is degraded to the red and shows two *R*-heads. Four branches of equal intensity could be picked out. They form two *R*- and two *P*-branches of a $^2\Sigma$–$^2\Sigma$ transition quite in agreement with the theory. The rotational analysis conforms with the presumed transition. We have also spectrograms on the 1,0 and 0,1 sequences, but, as is evident from Fig. 1*b*, overlapping from other bands makes the analysis of the 1,0 band rather unpromising, and the same applies to the 0,1 sequence.

In one of the *P*-branches of the 0,0 band of the $^2\Sigma$–$^2\Sigma$ system a slight perturbation was found. The analysis shows that the corresponding perturbation in the *R*-branch is concealed behind an atomic line.

The orange bands, which represent a $^2\Pi$–$^2\Sigma$ transition according to Johnson and Johnson, consist mainly of two marked sequences of equal intensity. These may therefore be regarded as the 0,0 sequences, representing $^2\Pi_{3/2}$–$^2\Sigma$ and $^2\Pi_{1/2}$–$^2\Sigma$ respectively. The structure of the bands in very dense. In spite of the large dispersion of the spectrograph the band heads are far from resolved. Hence the difference between the B-values in the upper and the lower states is probably very small. The computing of ΔB from the branches confirms this assumption. The separation of the two band groups is about 400 cm^{-1}, and consequently the term $^2\Pi$ belongs to Hund's case a. Thus the satellite branches will appear with the same strength as the main branches. The Q, ^RQ and ^PQ branches are twice as intense as the ^SR, R, ^QR, ^QP, P and ^OP branches, which have approximately equal intensity. A schematic figure of a $^2\Pi(a)$–$^2\Sigma$ transition is given in Fig. 4. Fig. 2 shows the appearance of the two sub-systems. If one adopts Johnson and Johnson's vibrational analysis, it is natural to assume that the weaker heads at $\lambda = 5939$ Å and $\lambda = 5956$ Å are formed either by ^SR branches or by R_1 branches according to whether the term $^2\Pi$ is regular or inverted. The stronger heads at $\lambda = 5972$ Å and so on must then represent the R_2 branch with the associated satellite $^RQ_{21}$ branch, or the Q_1 branch with the $^QR_{12}$ branch. As is seen from the figure, a distinct intensity minimum occurs in the "violet" 0,0 band at some distance from the Q-type head at $\lambda = 5972$ Å. Johnson and Johnson hesitated in their designation of the transition because of the unusually great distance between the presumed R- and Q-heads. However, this distance is fully explained by the small difference of the ΔB value mentioned above. The same arguments also hold for the other part of the 0,0 sequence (Fig. 2). The "red" band group shows almost the same structure as the "violet" one. Overlapping by the preceding band gives a less distinct appearance. Thus the heads at $\lambda = 6107$ Å and $\lambda = 6128$ Å are identical with higher members of the preceding "violet" sub-bands. The 0,1 and 1,0 bands are much weaker and are overlapped by other bands, and they are thus not suitable for rotational analysis. The 1,1 band is strong, but owing to almost total overlapping of all branches except the R_1 and ^SR branches, we cannot present a safe analysis.

The rotational structure and the course of the branches of the 0,0 bands are seen in Figs. 3a and 3b. Fig. 3a shows a slight perturbation in two branches. The perturbation is easily detectable in the non-overlapped ^SR branch ($N = 84$) but is very distinct also in the Q_2 branch ($N = 86$). On the assumption that the perturbation is in the upper state, second differences of the lower state could be obtained. These differences fitted very well both in the other sub-band of the orange system and in the blue-green system. Thus it is established that the two band systems have the lower state in common. The intensity minimum in the "violet" 0,0 band mentioned above simply turns out to be the region of the zero gap. No corresponding gap is seen in the "red" 0,0 band owing to overlapping by other bands.

Calculations of the first combination differences showed that no Λ-type doubling is present in the "violet" sub-band. The "red" sub-band shows a considerable Λ-type doubling, increasing linearly with J. The conclusion is that the $^2\Pi$ term of YO is regular, as the Λ-type doubling of $^2\Pi_{3/2}$ is much smaller than that of $^2\Pi_{1/2}$ according to the theory.

Blue-green system

Rotational analysis

The band lines are given in Table 1. Lines overlapped by other band lines or atomic lines are marked with an asterisk. The perturbation mentioned above occurs in P_2 (55). The F_2-level $N' = 54$ is thus slightly perturbed.

Table 1. Wave-numbers of $^2\Sigma$–$^2\Sigma$ (the 0,0 band).

N	R_1	P_1	R_2	P_2
23		20 717.37		20 714.19*
24		15.94		12.58*
25		14.47		10.96*
26		12.99		09.35*
27		11.42		07.70*
28		09.90*		05.95*
29		08.26*		04.23*
30	20 752.15	06.55*		02.44*
31	51.59	04.92		00.51
32	51.67	03.24		698.75
33	51.38	01.46	20 746.39*	96.83
34	51.08	699.68	45.92	94.91
35	50.75	97.91	45.44	92.98*
36	50.43	96.08	44.98*	90.95*
37	50.02	94.21	44.44	88.90*
38	49.56	92.31	43.87	87.01*
39	49.14	90.36	43.25	84.89*
40	48.65	88.39	atom	82.76*
41	48.10	86.36	41.95*	80.61*
42	47.57	84.40	41.25	78.40*
43	46.98	82.32*	40.56	76.19*
44	46.39*	80.14*	39.77	73.88*
45	45.68	78.09	38.97	71.54*
46	44.98*	75.98	38.18*	69.36*
47	44.27	73.71	37.26*	66.98*
48	43.54*	71.54*	36.24*	64.64*
49	atom	69.36*	35.47	62.27*
50	41.95*	66.98*	34.51	59.84*
51	41.05	64.64*	33.43	57.37
52	40.16	62.27*	32.41	54.80*
53	39.18	59.84	atom	52.28
54	38.18*	57.27	30.16	49.70
55	37.26*	54.80*	29.06	46.81
56	36.24*	52.47	27.90*	44.45
57	35.18	50.05	atom	41.77
58	34.13	47.43	25.40*	39.07
59	32.94	44.83	24.14	36.33
60	atom	42.23	22.87	33.53
61	30.61	39.53	21.51	30.71
62	29.28	36.81	20.13	27.92
63	27.90*	34.12	18.72	25.00
64	atom	atom	17.18	22.12
65	25.40*	28.54	15.70	19.21
66	23.93	25.69	14.19*	16.23
67	22.63	22.86	12.58*	13.15
68	21.15	19.92	10.96*	10.09
69	19.66	17.04	09.35*	07.07
70	18.12	14.02	07.70*	03.93
71	16.58	11.08	05.95*	00.81

Table 1 (cont.)

N	R_1	P_1	R_2	P_2
72	15.01	08.03	04.23*	597.64
73	13.37	04.89	02.44*	94.40
74	11.71	01.88	00.71	91.12
75	09.90*	598.74	698.99*	87.93
76	08.26*	95.55	97.04*	84.56
77	06.55*	atom	95.11*	81.19
78	04.71	89.10	93.15	77.84
79	02.87	85.84	91.16	74.41
80	00.99	82.50	89.07	atom
81	698.99*	79.19	87.01*	67.50
82	97.04*	75.84	84.89*	63.98
83	95.11*	72.34	82.76*	60.40
84	92.98*	68.91	80.61*	56.77
85	90.95*	65.48	78.40*	53.15
86	88.90*	61.92	76.19*	49.49
87	86.79	58.40	73.88*	45.82
88	84.65	54.78	71.54*	41.97
89	82.32*	51.21	69.15	38.27
90	80.14*	47.52	66.76	34.40
91	77.86	43.81	64.31	30.60
92	75.54	40.05	61.80	26.69
93	73.17	36.31	59.36	atom
94	70.77	32.48	56.76	atom
95	68.33	28.70	54.20	14.80
96	65.85	24.78	51.56	atom
97	63.33	20.84	48.90	06.72
98	60.80	16.96	46.17	02.66
99	58.19	12.91	43.41	498.47
100	55.39	08.92	40.76	94.28
101	52.90	atom	37.91	90.07
102		00.72	34.97	85.91
103		496.57	32.07	81.54
104		92.46	29.15	77.21
105		88.20	26.14	72.82
106		83.95	23.18	
107		79.63	20.09	
108		75.30		

Evaluation of constants

In the case of $^2\Sigma$ states the rotational term values are given by approximately

$$\left.\begin{aligned} F_1(N) &= BN(N+1) - DN^2(N+1)^2 + \tfrac{1}{2}\gamma N, \\ F_2(N) &= BN(N+1) - DN^2(N+1)^2 - \tfrac{1}{2}\gamma(N+1), \end{aligned}\right\} \qquad (1)$$

where $F_1(N)$ refers to the components with $J = N + \frac{1}{2}$ and $F_2(N)$ refers to those with $J = N - \frac{1}{2}$.

The B' and D' values are obtained graphically from the equation

$$\frac{\Delta_2 F_1'(J) + \Delta F_2'(J)}{2(J+\frac{1}{2})} = 4B' - 8D'(J+\tfrac{1}{2})^2. \tag{2}$$

These values, as well as all constants derived below, are given in the abstract. An estimate of α may be obtained from the expression by Pekeris [6]:

$$\alpha_e = \frac{6\sqrt{\omega_e x_e B_e^3}}{\omega_e} - \frac{6B_e^2}{\omega_e}.$$

As only the 0,0 band has been analysed no experimental value of α can be derived. The values obtained are given in Table 4.

The calculation of the constants of the lower state is treated in connection with the orange system.

Spin-splittings. From eq. (1) one obtains

$$F_1(N) - F_2(N) = \gamma(N+\tfrac{1}{2}). \tag{3}$$

Thus
$$\Delta_2 F_1''(N) - \Delta_2 F_2''(N) = 2\gamma''. \tag{4}$$

The $\Delta_2 F_1''(N)$ and $\Delta_2 F_2''(N)$ values have been calculated for every N-value available, and they agree within the accuracy of the measurements. The empirical mean value of γ'' is of the magnitude 0.001 cm^{-1}, but owing to the uncertainty of the measurements it is impossible to ascribe any definite value to γ''. Consequently we may put it equal to zero.

Assuming that $\gamma'' = 0$, the upper spin-splitting constant γ' has been calculated from

$$R_1(N-1) - R_2(N-1) = P_1(N+1) - P_2(N+1) = \gamma'(N+\tfrac{1}{2}).$$

The spin-splitting in $B\,^2\Sigma$ is very large, amounting to nearly 15 cm^{-1} at $N = 100$. In Fig. 5 the spin-splitting is plotted as a function of $(N+\frac{1}{2})$. The plot is not strictly linear, and a second-order term of the magnitude $\sim 5 \cdot 10^{-4}(N+\frac{1}{2})^2$ might be added.

Calculation of origin. The band origin was calculated with the formula

$$4\sigma_0 = R_1(N) + P_1(N+1) + R_2(N-1) + P_2(N) - 2(B' - B'')\,[N^2 + (N+1)^2].$$

If one plots the right-hand side expression (with an approximate ΔB value) against $N^2 + (N+1)^2$, $4\sigma_0$ is obtained as the intercept of the ordinate.

Orange system

Rotational analysis

The band lines are given in Table 2. The satellite branch $^PQ_{12}$ coincides with the P_1 branch in its full extension as does also the $^QR_{12}$ branch with the Q_1 branch. Analogous coincidences occur in the $^2\Pi_{3/2}$–$^2\Sigma$ sub-band. This fact supports our earlier assumption that γ'' is zero.

The level $J' = 85.5$ is perturbed, giving a displacement from the regular position of about 0.2 cm^{-1} in the lines ^SR (84) and Q_2 (86). No other perturbations have been found in the two sub-bands.

The combination differences of the lower state agree very well with the ones of the blue-green system, as is seen in Table 3.

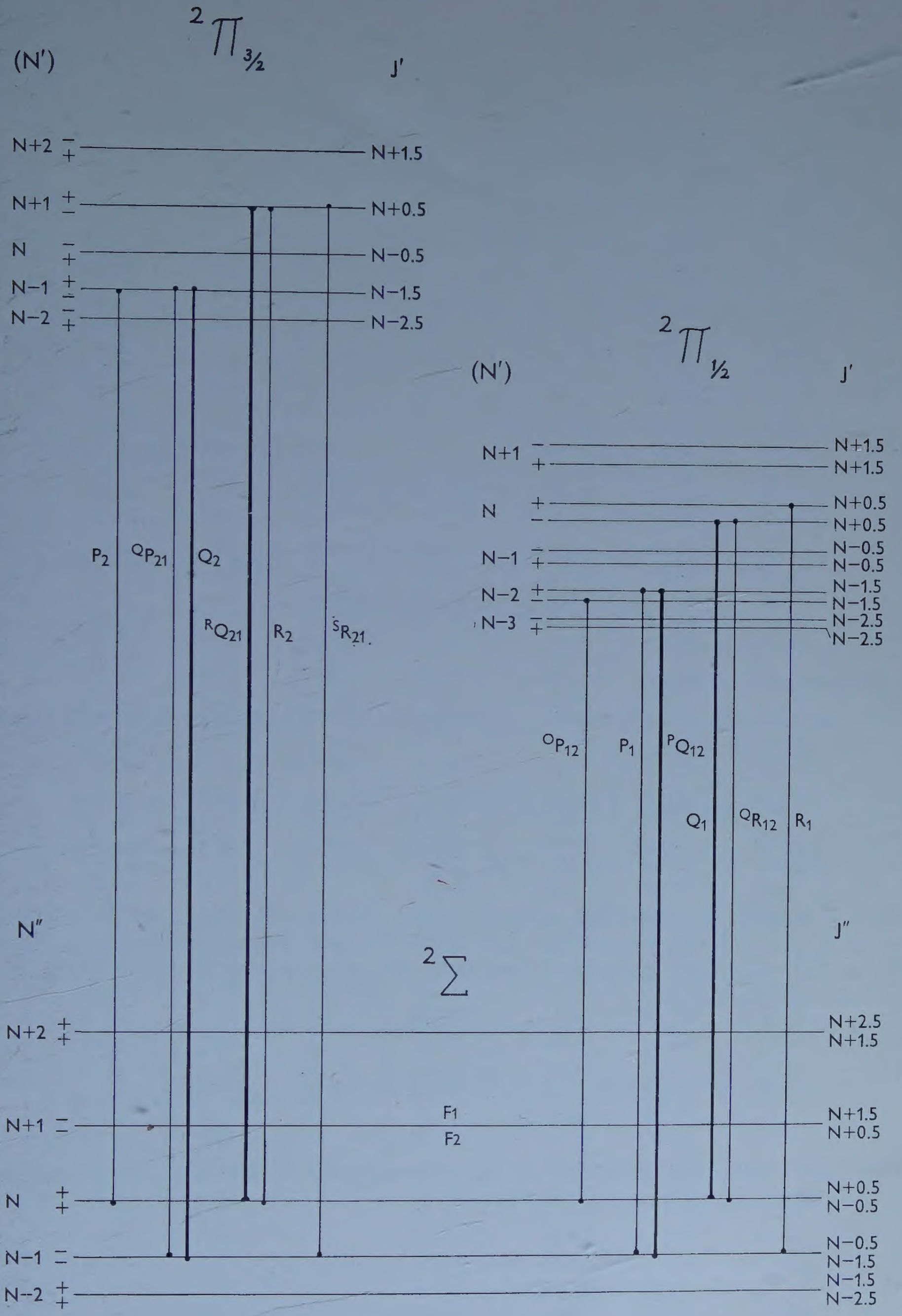

Fig. 4. $^2\Pi(a)$–$^2\Sigma$.

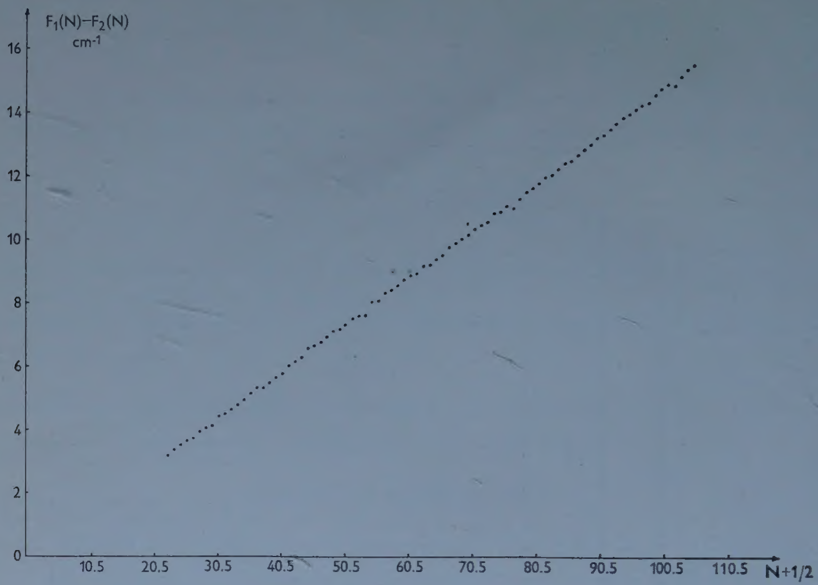

Fig. 5. The spin-splitting in $B\,{}^2\Sigma$ ($v = 0$).

Evaluation of constants

The rotational term values of the components of a ${}^2\Pi$-state have been calculated by Hill and Van Vleck [7].

$$F_1(J) = B\{(J+\tfrac{1}{2})^2 - \Lambda^2 - \tfrac{1}{2}\sqrt{4(J+\tfrac{1}{2})^2 + Y(Y-4)\Lambda^2}\} - DJ^4; \quad J = N + \tfrac{1}{2} \qquad (5)$$

$$F_2(J) = B\{(J+\tfrac{1}{2})^2 - \Lambda^2 + \tfrac{1}{2}\sqrt{4(J+\tfrac{1}{2})^2 + Y(Y-4)\Lambda^2}\} - D(J+1)^4; \quad J = N - \tfrac{1}{2}, \qquad (6)$$

where $Y = A/B$. In this case A amounts to approx. 400 cm^{-1}. As B is approx. 0.4 cm^{-1}, Y is of the magnitude 1000. The ${}^2\Pi$ term belongs evidently to Hund's case *a*. The multiplet splitting constant A is approximately equal to the distance between the sub-bands.

The B' and D' values are obtained graphically from the equation

$$\frac{\Delta_2 F'_{1c}(J) + \Delta_2 F'_{1d}(J) + \Delta_2 F'_{2c}(J) + \Delta_2 F'_{2d}(J)}{4(J+\tfrac{1}{2})} = 4B' - 8D'(J+\tfrac{1}{2})^2.$$

The lower rotational constants are derived from the six sets of $\Delta_2\, F''(N)$ values of ${}^2\Sigma$–${}^2\Sigma$ and ${}^2\Pi$–${}^2\Sigma$. From eq. (1) we have:

$$\frac{\Delta_2 F''(N)_{\text{mean}}}{N+\tfrac{1}{2}} = 4B'' - 8D''(N+\tfrac{1}{2})^2,$$

provided that $\gamma'' = 0$. α' and α'' can be calculated from Pekeris' formula [6]. The values obtained are collected in Table 4.

Table 2. Wave-numbers of $^2\Pi$–$^2\Sigma$ (the 0,0 band)

N	$^2\Pi_{1/2}$–$^2\Sigma$				$^2\Pi_{3/2}$–$^2\Sigma$			
	R_1	$P_1+{}^PQ_{12}$	$Q_1+{}^QR_{12}$	${}^OP_{12}$	${}^SR_{21}$	$Q_2+{}^QP_{21}$	$R_2+{}^RQ_{21}$	P_2
6	16 303.66						16 725.21	16 715.68
7	04.82						25.60	14.55*
8	06.04					16 719.18	25.94	13.62*
9	07.08					18.91	26.29	12.44
10	08.41					18.52	26.61	11.24*
11	09.53					18.09	26.97	09.98
12	10.69					17.70	27.32	08.75*
13	11.85					17.22	27.69	07.61
14	13.01					16.82	27.99	06.36
15	14.13				16 741.08	16.37	28.31	05.12*
16	15.25	16 288.96	16 299.13*		42.16	15.90	28.70	04.04
17	16.42	88.55	99.36*		43.25	15.46	28.95	02.69
18	17.56	88.17*	99.59*	16 272.00*	44.33	14.99	29.24	01.49
19	18.68	87.68*	99.81*	70.78*	45.41	14.55*	29.62	00.29
20	19.80	87.32	00.02*	69.36	46.50	14.06	29.90	699.11
21	20.90	86.87	00.23*	68.02	47.57	13.62*	30.23	97.81*
22	22.02	atom	00.42*	66.67	48.65	13.15	30.51	96.68*
23	23.13	86.01*	00.66*	65.30	49.71	12.67	30.81	95.43*
24	24.23	85.57	00.84*	63.94	50.77	12.20	31.10	94.18*
25	25.30	85.12	01.03*	62.56	51.78	11.75	31.34	92.92*
26	26.37	84.66	01.19*	61.19	52.88	11.24*	31.69	91.68*
27	27.50	84.20	01.35*	head	53.96	10.73	31.95	90.40*
28	28.51	83.72*	01.51*	58.55	54.98	10.24	32.23	89.12*
29	29.56	83.27	01.66*	57.25*	56.01	09.75	32.49	87.80*
30	30.63	82.79	01.79*	55.75*	57.06	09.25	32.78	86.46*
31	31.68	82.30	01.91*	54.34	58.09	08.75*	33.04	85.23
32	32.71	81.83*	02.04*	53.07	59.09	08.24	33.29	83.97
33	33.74	81.28*		51.63	60.14	07.73	33.53	82.72
34	34.75	80.83		50.29*	61.14	07.21	33.81	81.38
35	35.82	80.32		48.79	62.18	06.69	34.04	80.15*
36	36.83	79.77		47.38	63.17	06.18	34.28	78.82
37	37.79	79.27*		45.92	64.19	05.66	34.50	77.57
38	38.81	78.76		44.44*	65.19	05.12*	34.76	76.22
39	39.84	78.22		42.86	66.21	04.58	35.00	74.94*
40	40.84	77.69		41.40	67.18	04.03	35.20	73.60
41	41.81	77.15*		atom	68.17	03.45	35.41	72.28
42	42.80	76.60		38.47	69.16	02.94	35.63	71.04*
43	43.77	76.04		36.99	70.12	02.39	35.86	69.63
44	44.71	75.49		35.51*	71.09	01.84	36.07	68.30
45	45.68	74.93		34.05	72.07	01.27	36.25	67.01*
46	46.64	74.35		32.59*	73.00	00.70	36.43	65.69
47	47.58	73.77		31.09	73.95	00.14	36.64	64.33
48	48.52	73.18		29.60	74.92	699.55	36.84	63.01
49	49.50	72.60		28.09	75.88	98.98	37.02	61.65
50	50.38	72.00*		26.58	76.81	98.40	37.19	60.31
51	51.31	71.39		25.06	77.76	97.81*	37.34	59.00
52	52.24	70.78*		23.57*	78.68	97.23	37.51	57.60
53	53.09	70.18		22.04	79.60	96.68*	37.68	56.24
54	53.99	69.54		20.44*	80.54	96.05	37.85	54.86

Table 2 (cont.)

N	$^2\Pi_{1/2}-^2\Sigma$				$^2\Pi_{3/2}-^2\Sigma$			
	R_1	$P_1+{}^PQ_{12}$	$Q_1+{}^QR_{12}$	${}^QP_{12}$	${}^SR_{21}$	$Q_2+{}^QP_{21}$	$R_2+{}^RQ_{21}$	P_2
55	54.89	68.91		18.95	81.43	95.43*	38.01	53.53
56	55.77	68.28		17.39	82.36	94.83		head
57	56.64	67.65		head	83.25	94.18*		50.72
58	57.52	67.01		14.23	84.19	93.59		49.38
59	58.37	66.35		12.66*	85.03	92.92*		48.00*
60	59.24	65.69		11.17	85.92	92.32		46.58
61	60.06	65.02		09.55	86.80	91.68*		45.19
62	60.90	64.35		08.10*	87.67	91.06		43.77
63	61.73	63.67		06.51	88.54	90.40*		42.42
64	62.54	62.99		04.90	89.40	89.76		41.10
65	63.35	62.29		03.28	90.25	89.12*		39.57
66	64.16	61.60		01.68	91.11	88.47		38.16
67	64.95	60.89		00.05	91.95	87.80*		36.74
68	65.75	60.18		198.39	92.79	87.11		35.35
69	66.52	head	16 302.04*	96.74	93.62	86.46*		33.83
70	67.28	58.70	01.91*	95.19	94.44	85.76		32.42
71	68.09	57.95	01.79*	93.58	95.26	85.08		31.00
72	68.83	57.25*	01.66*	91.92	96.06	84.40		29.54
73	69.58	56.50	01.51*	90.22	96.88	83.74		28.11
74	70.32	55.75*	01.35*	88.60	97.67	83.02		26.68
75	71.06	54.98	01.19*	86.93	98.47	82.30		25.18
76	71.78	54.23	01.03*	85.29	99.26	81.58		23.74
77	72.50	53.43	00.84*	83.60	800.04	80.87		22.28
78	73.21	52.69	00.66*	81.96	00.80	80.15*		20.78
79	73.91	51.88	00.42*	80.22	01.57	79.43		19.40
80	74.59	51.08	00.23*	78.49	02.32	78.69		17.85
81	75.25	50.29*	00.02*	76.75	03.08	77.96		16.33
82	75.95	49.47	299.81*	75.01	03.81	77.20		14.79
83	76.60	48.65	99.59*	73.42	04.53	76.45		13.29
84	77.28	47.84	99.36*	71.71	05.16	75.69		11.82
85	77.93	46.96	99.13*	69.97	06.08	74.94*		10.30
86	78.56	46.15	98.86	68.17	06.75	74.05		08.87
87	79.19	45.31	98.58		07.47	73.47		07.50
88	79.80	44.44*	98.31		08.16	72.66		05.94
89	80.43	43.58	98.04		08.85	71.84		04.38
90	81.03	42.72	97.77		09.53	71.04*		02.85
91	81.62	41.85	97.48		10.21	70.27		01.33
92	82.22	40.96	97.17		10.88	69.46		599.63
93	82.78	atom	96.83		11.54	68.64		98.08
94	83.35	39.13	96.52		12.19	67.83		96.60
95	83.92	38.24	96.19		12.84	67.01*		95.03
96	84.45	37.32	95.85		13.47	66.20		93.45
97	84.98	36.42	95.53		14.18*	65.33		92.00
98	85.50	35.51*	95.16		14.72	64.50		90.54
99	86.02	34.48	94.82		15.32	63.59		89.02
100	86.52	33.61	94.43		15.93	62.78		87.34
101	87.06	32.59*	94.05		16.54	61.90		85.67
102	87.53	31.65	93.65		17.11	61.05		83.89
103	87.99	30.66	93.24		17.69	60.18		82.48
104	88.43	29.72	92.85		18.26	59.29		80.68

ble 2 (cont.)

N	$^2\Pi_{1/2}$–$^2\Sigma$				$^2\Pi_{3/2}$–$^2\Sigma$			
	R_1	$P_1 + {}^PQ_{12}$	$Q_1 + {}^QR_{12}$	${}^QP_{12}$	${}^SR_{21}$	$Q_2 + {}^QP_{21}$	$R_2 + {}^RQ_{21}$	P_2
105	88.93	28.69	92.41		18.82	58.41		79.17
106	89.36	27.68	91.97		19.37	57.47		77.54
107	89.79	26.66	91.54		19.91	56.61		75.93
108	90.20	25.66	91.09		20.44	55.66		
109	90.63	24.61	90.62		20.95	54.75		
110	91.02	23.57*	90.16*		21.47	53.81		
111	91.42	22.55	89.71		21.99	52.89		
112	91.81	21.48	89.19		22.47	head		
113	92.18	20.44*	88.70		22.96	50.98		
114	92.54	19.35	88.17*		23.44	50.00		
115	92.89	18.28	87.68*		23.90	49.00		
116	93.21	17.18	87.12		24.36	48.00*		
117	93.54	16.13	86.59		24.81	46.96		
118	93.82	14.95	86.01*		25.23	45.86		
119	94.15	13.79	85.46		25.66	44.76		
120	94.41	12.66*	84.50		26.09			
121	94.74	11.61	84.31		26.48			
122	95.01	10.44	83.72*		26.87			
123	95.24	09.21	83.11		27.24			
124	95.48	08.10*	82.51		27.62			
125	95.70	06.93	81.83*		27.96			
126	95.93	05.68	81.28*		28.33			
127	96.10	04.38	80.58		28.68			
128	96.32		79.87		29.00			
129	96.52		79.27*		29.30			
130	96.66		78.55		29.61			
131	96.85		77.86		29.90			
132	96.98		77.15*		30.19			
133	97.13		76.42		30.47			
134	97.31		75.70		30.72			
135					30.96			
136					31.18			
137					31.39			
138					31.62			
139					31.82			
140					32.01			
141					32.17			
142					32.34			

It must again be pointed out that the B_e and r_e values are not based on experimental data but are merely approximate figures.

Λ-type doubling. The Λ-type doubling of a $^2\Pi$ state has been theoretically treated by Van Vleck [8]. In Hund's case *a* the doubling of the $^2\Pi_{1/2}$ state is equal to $a\,(J+\frac{1}{2})$ for not too large J-values, with the coefficient a approximately proportional to A, the multiplet splitting constant. For the $^2\Pi_{3/2}$ state the Λ-type splitting becomes smaller with increasing $|A|$, and is experimentally too small to be measured if $|A|$

Table 3. Some $\Delta_2 F''(N)$-values of $X^2\Sigma$ ($v''=0$).

N	From $^2\Sigma$–$^2\Sigma$		From $^2\Pi_{1/2}$–$^2\Sigma$		From $^2\Pi_{3/2}-{}^2\Sigma$	
	$R_1(N-1)$ $-P_1(N+1)$	$R_2(N-1)$ $-P_2(N+1)$	$R_1(N-1)$ $-P_1(N+1)$	$Q_1(N-1)$ $-{}^OP_{12}(N+1)$	${}^SR_{21}(N-1)$ $-Q_2(N+1)$	$R_2(N-1)$ $-P_2(N+1)$
30	—	—	47.26	47.32	47.26	47.26
35	55.00	54.97	54.98	—	54.96	54.99
40	62.78	62.64	62.69	—	62.76	62.72
45	70.41	70.41	70.36	—	70.39	70.38
50	—	78.10	78.11	—	78.07	78.02
55	85.71	85.71	85.71	—	85.71	—
60	93.41	93.43	93.35	—	—	—
65	—	100.95	100.94	—	100.93	—
70	108.58	108.54	108.57	108.46	108.54	—
75	116.16	116.15	116.09	116.06	116.09	—
80	123.68	123.66	123.62	123.67	123.61	—
85	131.06	131.12	131.13	131.19	131.11	—
90	138.51	138.55	138.58	—	138.58	—
95	145.99	—	146.03	—	145.99	—
100	—	153.34	153.43	—	153.42	—

Table 4.

	$X\,^2\Sigma$	$A\,^2\Pi$	$B\,^2\Sigma$
α cm^{-1}	0.0016	0.0019	0.0039
B_e cm^{-1}	0.3873	0.3847	0.3702
r_e Å	1.788	1.792	1.823

is fairly large. The width is proportional to $(J-\frac{1}{2})(J+\frac{1}{2})(J+\frac{3}{2})$ in a true case *a*.

The experimental results for the $A\,^2\Pi$ state of YO are quite in agreement with the theory. In the $^2\Pi_{3/2}$ state the first combination differences show that no Λ-type doubling is present while the $^2\Pi_{1/2}$ state shows considerable splitting. The Λ-type splitting in the level J is here denoted $\varepsilon(J)$.

$$\varepsilon(J)=\varepsilon(N+\tfrac{1}{2})=a(J+\tfrac{1}{2}).$$

$\varepsilon(J)$ is computed from a mean value of the following expressions (see Fig. 4).

$$\varepsilon(J)=P_1(N+1)-{}^OP_{12}(N+2)-\frac{\{{}^SR_{21}(N+1)-R_2(N+2)\}+\{{}^QP_{21}(N+1)-P_2(N+2)\}}{2}$$

$$\varepsilon(J)=R_1(N-1)-{}^QR_{12}(N)-\frac{\{{}^SR_{21}(N-1)-R_2(N)\}+\{{}^QP_{21}(N-1)-P_2(N)\}}{2}$$

Fig. 6 shows that the $\varepsilon(J)$ increases strictly proportionally to $J+\frac{1}{2}$ even for high J-values.

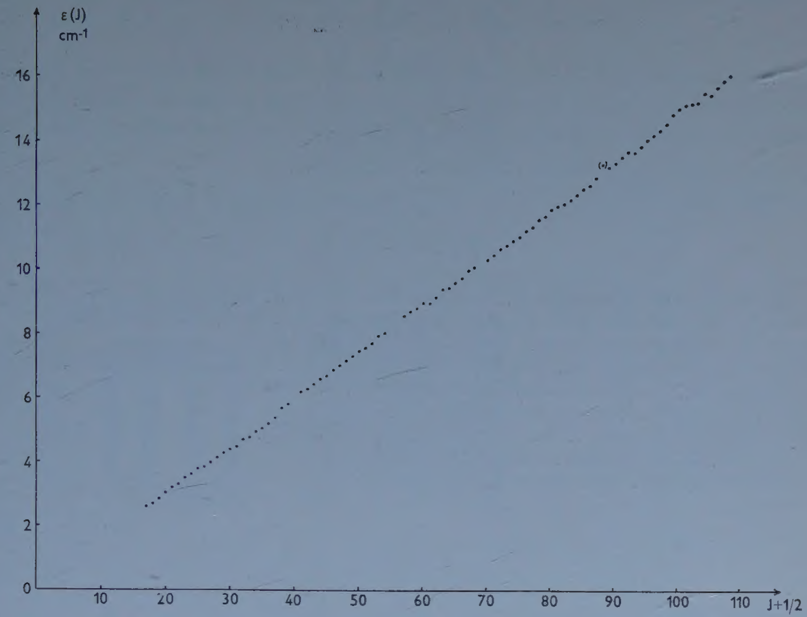

Fig. 6. The Λ-type doubling in $A\,^2\Pi_{1/2}(v=0)$.

Calculation of the origins. As mentioned above, the coupling constant Y is about 1000. In such a pronounced case a the square root in the energy expressions (5) and (6) may be replaced simply by Y. This approximation gives the formulas for the total energies, including also the Λ-type doubling:

$$\left.\begin{aligned} T_{1c}(J) &= W_1 - \frac{A}{2} + \tfrac{1}{2}a(J+\tfrac{1}{2}) + BJ(J+1) + \ldots, \\ T_{1d}(J) &= W_1 - \frac{A}{2} - \tfrac{1}{2}a(J+\tfrac{1}{2}) + BJ(J+1) + \ldots, \\ T_{2c}(J) = T2_d(J) &= W_2 + \frac{A}{2} + BJ(J+1) + \ldots, \end{aligned}\right\} \qquad (7)$$

The notations used above are those of Mulliken [9].

With the above formulas and eq. (1) the following expressions can be verified.

$$4\sigma_1 - 5B'' = R_1(N-1) + Q_1(N) + P_1(N+1) + {}^{O}P(N+2) - 4(B'-B'')\,\{(N+1)^2 - \tfrac{1}{4}\}$$

$$4\sigma_2 - 5B'' = {}^{S}R(N-2) + R_2(N-1) + Q_2(N) + P_2(N+1) - 4(B'-B'')(N^2 - \tfrac{1}{4}),$$

where σ_1 and σ_2 represent the origins of the two sub-bands.

If one plots the right-hand side expressions (using an approximate ΔB value) against $\{(N+1)^2 - \frac{1}{4}\}$ and $(N^2 - \frac{1}{4})$ respectively, and extrapolates to zero, one obtains the origins.

Multiplet splitting. The multiplet splitting constant A is obtained simply by subtracting $\sigma_2 - \sigma_1$ as a consequence of the approximate energy expressions (7).

ACKNOWLEDGEMENTS

We wish to express our gratitude to Professor Erik Hulthén for his kindness in placing at our disposal his immersion grating spectrograph, whose superior properties have made this investigation possible. We are also indebted to F. M. Bengt Yttermo for his careful experimental help.

Physics Department, University of Stockholm. May 1960.

REFERENCES

1. MEGGERS, W. F., and WHEELER, J. A., Nat. Bur. Stand. J. Research, *6*, 239 (1931).
2. JOHNSON, L. W., and JOHNSON, R. C., Proc. Roy. Soc. London A *133*, 207 (1931).
3. HULTHÉN, E., and NEUHAUS., H., Arkiv f. Fysik *8*, 343 (1954).
4. HULTHÉN, E., JOHANSSON, N., and PILSÄTER, U., Arkiv f. Fysik, *14*, 31 (1958).
5. LUNDEGÅRDH, H., Lantbrukshögskolans annaler *3*, 49 (1936).
6. PEKERIS, C. L., Phys. Rev. *45*, 98, 1934.
7. HILL, E., and VAN VLECK, J. H., Phys. Rev. *32*, 250 (1928).
8. VAN VLECK, J. H., Phys. Rev. *33*, 467 (1929).
9. MULLIKEN, R. S., Rev. Mod. Phys. *3*, 129 (1931).

Tryckt den 27 januari 1961

Uppsala 1961. Almqvist & Wiksells Boktryckeri AB